Journal of Alloys and Compounds 509 (2011) 9413–9418

Contents lists available at ScienceDirect

Journal of Alloys and Compounds

journal homepage: www.elsevier.com/locate/jallcom

The effect of texture and strain conditions on formability of cross-roll rolled AZ31 alloy

Dae-Guen Kim[a,b,*], Hyeon-Taek Son[a], Dae-Won Kim[a], Young-Ho Kim[a], Kye-Man Lee[b]

[a] Korea Institute of Industrial Technology, 1110-9 Oryong-dong, Buk-gu, Gwangju 500-480, Republic of Korea
[b] Department of Materials Science and Engineering, Korea University, Anam-dong 5-1, Seongbuk-gu, Seoul 136-713, Republic of Korea

ARTICLE INFO

Article history:
Received 23 May 2011
Received in revised form 6 July 2011
Accepted 7 July 2011
Available online 18 July 2011

Keywords:
AZ31 sheet
Cross-roll rolling
X-ray diffraction
Three-dimensional finite element method
Texture

ABSTRACT

The effect of texture evolution of AZ31 Mg sheet on cross-roll rolling process has been investigated for the commercial AZ31 Mg sheet. The large ε_{23} was operated for the cross-roll rolled sample throughout the whole thickness, leading to the homogeneity of the (0002) basal texture. After recrystallization annealing at 673 K for 30 min, cross-roll rolled sample showed uniform texture intensity from surface layer to middle layer different from the normal-roll rolled sample. An excellent formability of the cross-rolled specimen was achieved due to the developed homogeneity of the texture and microstructure refinement for the cross-roll rolled specimen. The strain conditions of surface and center layers were discussed in terms of experimental evaluations and three-dimensional finite element method (FEM) for conventional rolling and cross-roll rolling.

1. Introduction

Mg alloys are one attractive material in applications of transportations and mobile electronics [1], because of their low densities and high specific strength [2]. However, Mg alloys often exhibit relatively low strength and poor formability at room temperature [3]. The limited ductility is attributed to a strong planar anisotropy, where the basal plane (0002) tends to be distributed parallel to the rolling direction, since the basal slip mode provides the only two independent slip systems [4–6]. However, it has been reported that both ductility and texture of Mg alloys during rolling process largely depend on rolling conditions such as rolling temperature, rolling direction and plastic deformation [7]. For example, warm forming can improve the formability of magnesium alloy, because the pyramidal plane of Mg crystal structure is operated by thermal activation during deformation [8]. The microstructure and mechanical properties and texture evolution of Mg alloys are highly dependent on their primary deformation process such as cross rolling [9], different speeds-rolling [10], ECAP [11] and ECAR [12]. In particular, cross-roll rolling is expected to improve the grain refinement, mechanical properties and formability.

For the cross-roll rolling process, the operation of the shear deformation along TD (transverse direction) is expected, because the thrust force in an axial direction of a roll can be imposed on a rolled sheet. Since the rolls are crossed in the RD–TD plane, the rolling process has been referred to as "cross-roll" rolling in order to distinguish it from the conventional cross-rolling process, in which the RD (rolling direction) is rotated after each rolling pass [13–16]. Chino et al. reported that the cross-roll rolling is effective for the imposition of severe shear straining on rolled materials, leading to an improvement of microstructure and formability of magnesium alloy sheets [14–18]. Since cross-roll rolling leads to the formation of a deformation microstructure different from that obtained during normal rolling, the deformation during cross-roll rolling is distinguished from those during conventional normal rolling. Therefore, it is manifested that the identification of strain state during cross-roll rolling can provide a significant insight for understanding cross-roll deformation, so that control of the strain state can be used for practical application. However, the evolution of microstructures and the resultant strain state during cross-roll rolling has not been scrutinized, while structural features have been relatively well reported [9,15].

In the present study, the evolution of strain states during cross-roll rolling was investigated and the strain conditions were identified along the stream lines through the thickness layers by three-dimensional finite element method (FEM). At the same time, in order to understand the strain mode difference between conventional rolling and cross-roll rolling, the microstructure and textures evolution were distinctly investigated for the commercial AZ31 alloy.

* Corresponding author at: Korea Institute of Industrial Technology, 1110-9 Oryong-dong, Buk-gu, Gwangju 500-480, Republic of Korea. Tel.: +82 62 6006291; fax: +82 62 6006149.
E-mail addresses: dgkim7@kitech.re.kr, deonkin@korea.ac.kr (D.-G. Kim).

0925-8388/$ – see front matter © 2011 Elsevier B.V. All rights reserved.
doi:10.1016/j.jallcom.2011.07.013

Table 1
The chemical composition(wt.%) of the initial AZ31 alloys sheet.

Mg	Al	Zn	Mn	Si	Fe	Cu	Ni
Blaance	3.1	1.0	0.41	<0.01	0.0023	<0.01	0.0023

2. Experimental procedures

The material used in this study was commercial AZ31 alloy. The initial specimen size was about 70 mm × 70 mm × 4 mm (width, length and thickness). The chemical compositions of AZ31 alloy sheet are listed in Table 1. Schematic view of rolling routes for (a) normal rolling and (b) cross-roll rolling is shown in Fig. 1. Cross-roll rolling with 75% of total reduction ratio was conducted at 673 K, where the roll axis was tilted by normal rolling and 7.5° against TD in the RD–TD plane. The rolled Mg alloy sheets were annealed at 673 K for 30 min. The each pass treatments at 673 K for 20 min were repeated several times, and finally, the sheets were rolled to a thickness of 1.0 mm and the total reduction was about 75%. For comparison, the normal-roll rolling was conducted under the same rolling schedule. In order to adjust

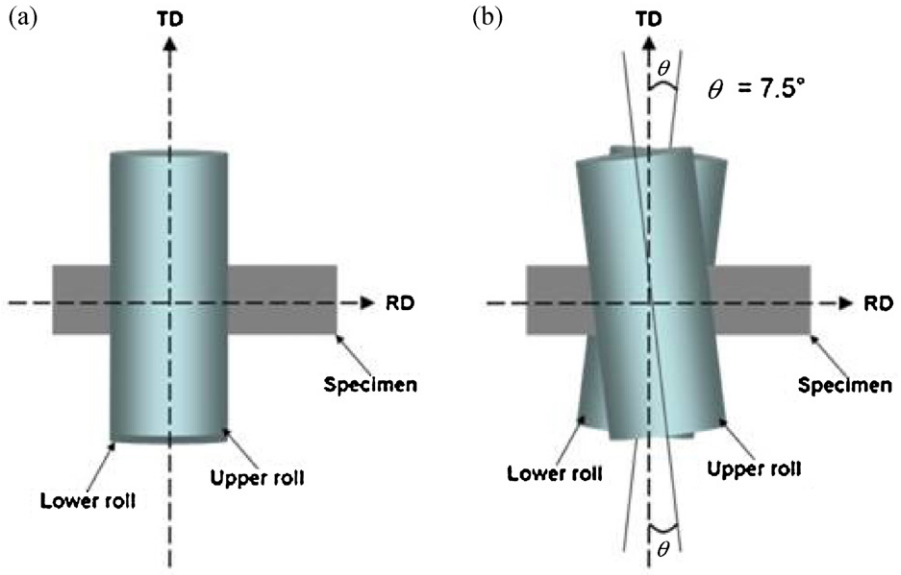

Fig. 1. Schematic view of rolling routes for the cross-roll rolling.

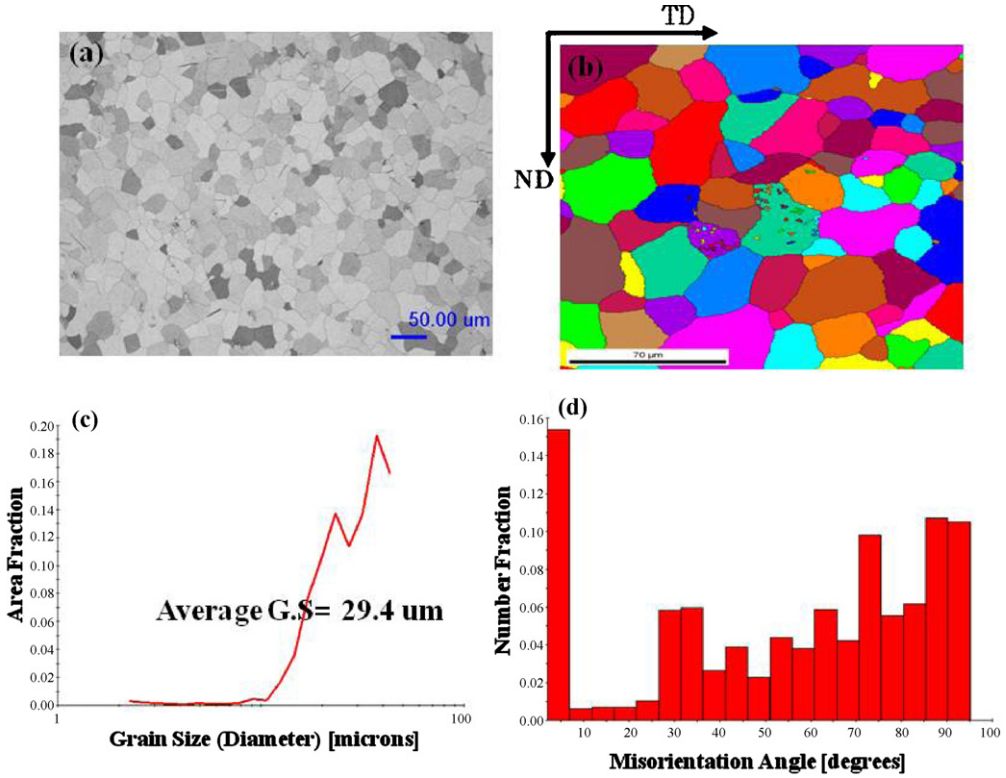

Fig. 2. (a) Optical microstructure; (b) inverse pole figure maps (IPF); (c) average grain size; (d) Frequency-misorientation map of the as-received sheet.

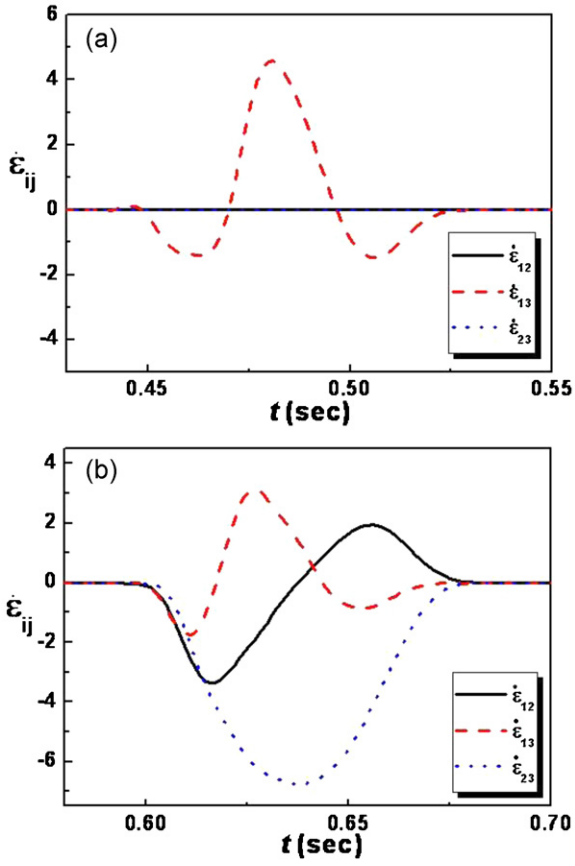

Fig. 3. Variation of shear strain rate components, at surface layer during (a) normal rolling and (b) cross-roll rolling.

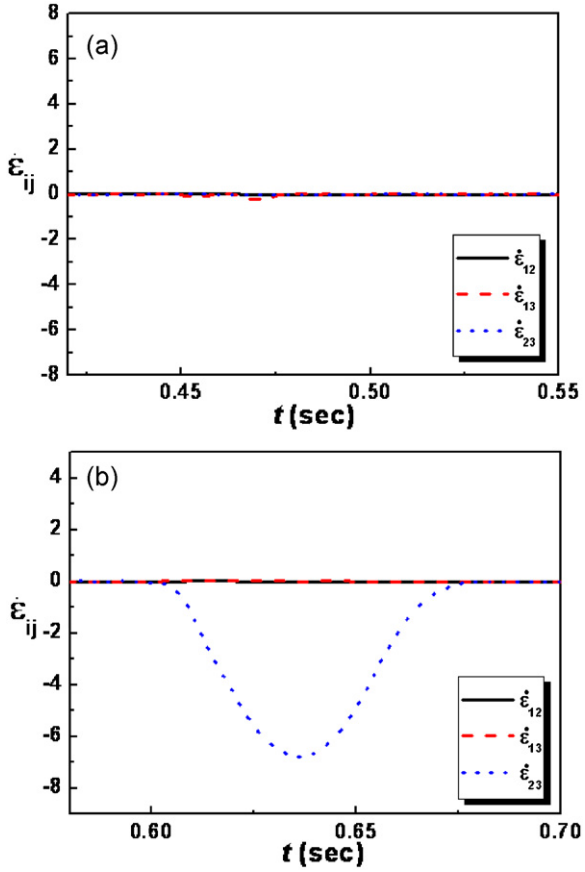

Fig. 4. Variation of shear strain rate components, at center layer during (a) normal rolling and (b) cross-roll rolling.

the grain size, heating condition of the specimens before rolling was set to 673 K for 20 min. The rolling procedure was the same as those of the specimens by the cross-roll rolling. Microstructures of the rolled Mg alloy sheets were investigated by scanning electron microscopy (SEM). Grain size and texture of cross-roll rolled and normal rolled specimens were determined by electron back scattering diffraction (EBSD) and X-ray diffraction with CoKα radiation up to a tilt angle of 70° using the Schultz reflection method. The EBSD software was provided by TSL Technology®. In order to interpret the distributions of strain states in the roll gap during cross-roll rolling, the three-dimensional finite element method (FEM) simulations were used, i.e. the rigid-plastic FEM code DEFORM. For the FEM calculation, the friction parameter m was used, where m is defined as the ratio of the frictional stress to the critical stress, and $m = 1$ denotes sticking. Because a high friction without lubrication prevailed during rolling without lubrication, the value of m between the sample surface and rolls was assumed as 0.6. At the same time, Since the strain state is strongly dependent on the whole sample thickness, the textures of the surface and center parts were separately investigated after the cross-roll rolling. In order to denote the position of the sheet cross section (i.e., the center or the surface of the sheet), the location of the sheet cross section was characterized by the parameter s (0.0–1.0), where $s = 1.0$ denotes the surface and $s = 0.0$ does the center of the sheet cross section.

3. Results and discussion

Fig. 2(a) and (b) shows the microstructure of the RD–TD of the initial sheet. It is observed that the microstructure is very homogeneous and composed of equiaxed grains. The average grain size was ~29.4 μm measured by the electron backscatter diffraction (EBSD). Fig. 2(d) shows the frequency–misorientation map of the as-received sheet. The frequency values of high angle grain boundaries (HAGB > 15°) and low angle grain boundaries (LAGB < 15°) was detected by EBSD method were 83% and 17%, respectively, which were detected by EBSD method.

The variation of strain states in the roll gap during normal and cross-roll rolling was investigated by three-dimensional finite element method (FEM) simulations using the rigid-plastic FEM code DEFORM for the surface and central part of the sheet cross section. Fig. 3 shows variations of shear–strain rates $\dot{\varepsilon}_{12}$, $\dot{\varepsilon}_{13}$ and $\dot{\varepsilon}_{23}$ in the roll gap along the stream line at the sheet surface during normal rolling (Fig. 3(a)) and cross-roll rolling (Fig. 3(b)). During normal rolling, only the component $\dot{\varepsilon}_{13}$ varies and other components $\dot{\varepsilon}_{12}$ and $\dot{\varepsilon}_{23}$ are zero at the surface of the sheet. As reported earlier [19–21], the operation of large shear component $\dot{\varepsilon}_{13}$ during normal rolling leads to the formation of shear textures. In contrast, all three shear components $\dot{\varepsilon}_{12}$, $\dot{\varepsilon}_{13}$ and $\dot{\varepsilon}_{23}$ are largely and independently changed in the roll gap during the cross-roll rolling process (Fig. 3(b)). Variations of shear strain rates $\dot{\varepsilon}_{12}$, $\dot{\varepsilon}_{13}$ and $\dot{\varepsilon}_{23}$ in the roll gap along the stream line of the sheet center are shown in Fig. 4. For the central part of the normally rolled sheet, all shear–strain rates are nearly zero in the roll gap, i.e. it showed conventional plane strain condition. The center layer of the cross-roll rolled sheet displays a large variation of $\dot{\varepsilon}_{23}$, while other strain components $\dot{\varepsilon}_{12}$ and $\dot{\varepsilon}_{13}$ are zero (Fig. 4(b)). The similar variation of $\dot{\varepsilon}_{23}$ is observed in the whole thickness of the cross-roll rolled sample, while the effect of the $\dot{\varepsilon}_{23}$ strain is not critically operated for the cross rolled specimen.

Fig. 5 shows the microstructures of the rolled AZ31 alloys: (a) normal rolling sample before annealing, (b) normal rolling samples after annealing at 473 K for 30 min, (c) cross-roll rolling sample before annealing, (d) cross-roll rolling samples after annealing at 473 K for 30 min. The twins were observed for the normal and cross-roll rolling processes before the annealing heat treatments. Also, the microstructural observations showed that more twins were observed at cross-roll rolling sample, compared with Fig. 5(a) and (c). Also, in order to examine the effect of heat treatments, both sheets were annealed at 673 K for 30 min. The average grain sizes

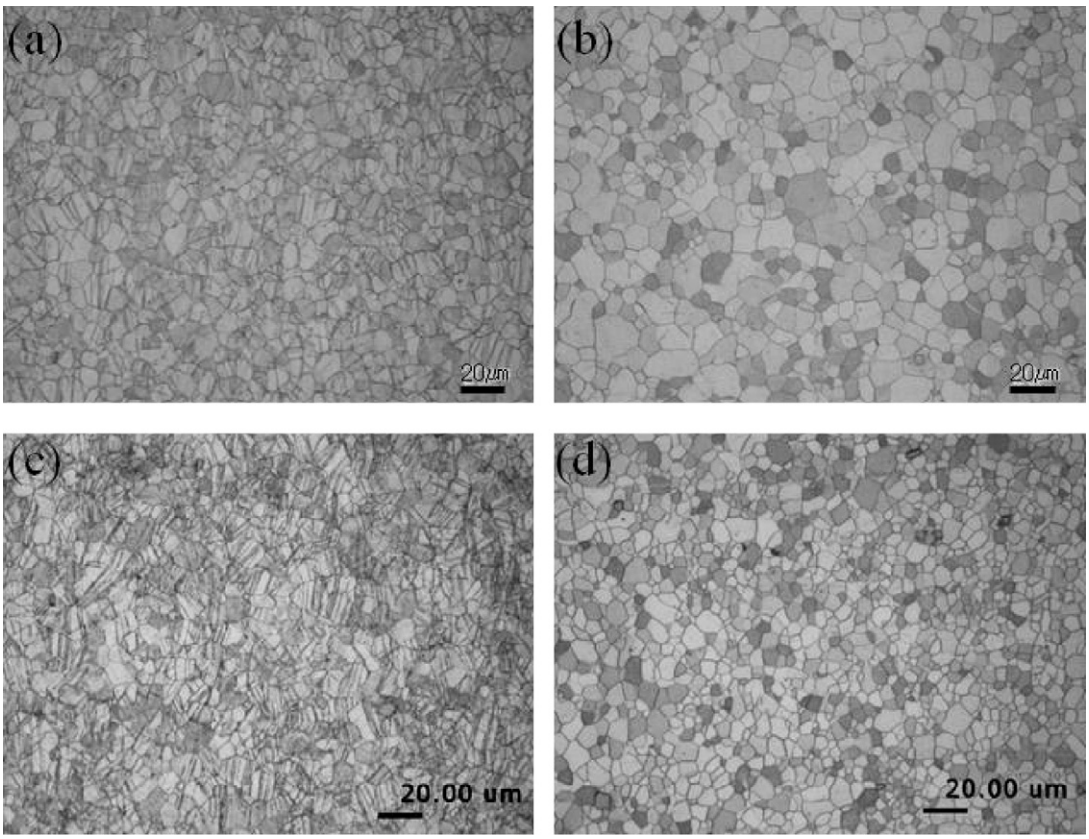

Fig. 5. The microstructure of the rolled AZ31 alloys: (a) normal rolling sample before annealing, (b) normal rolling samples after annealing at 473 K for 30 min, (c) cross-roll rolling sample before annealing, and (d) cross-roll rolling samples after annealing at 473 K for 30 min.

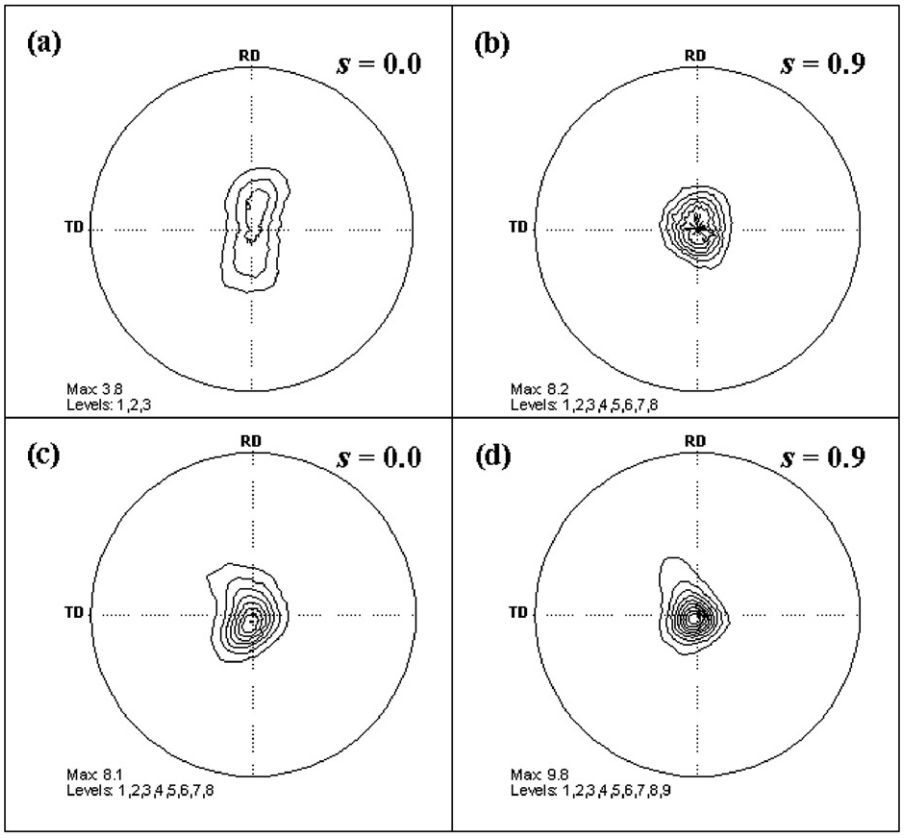

Fig. 6. (0 0 0 2) pole figures of the rolled AZ31 alloys: (a and b) normal rolling samples, and (c and d) cross-roll rolling samples ($s = 0.0$ is center layer; $s = 0.9$ is surface layer).

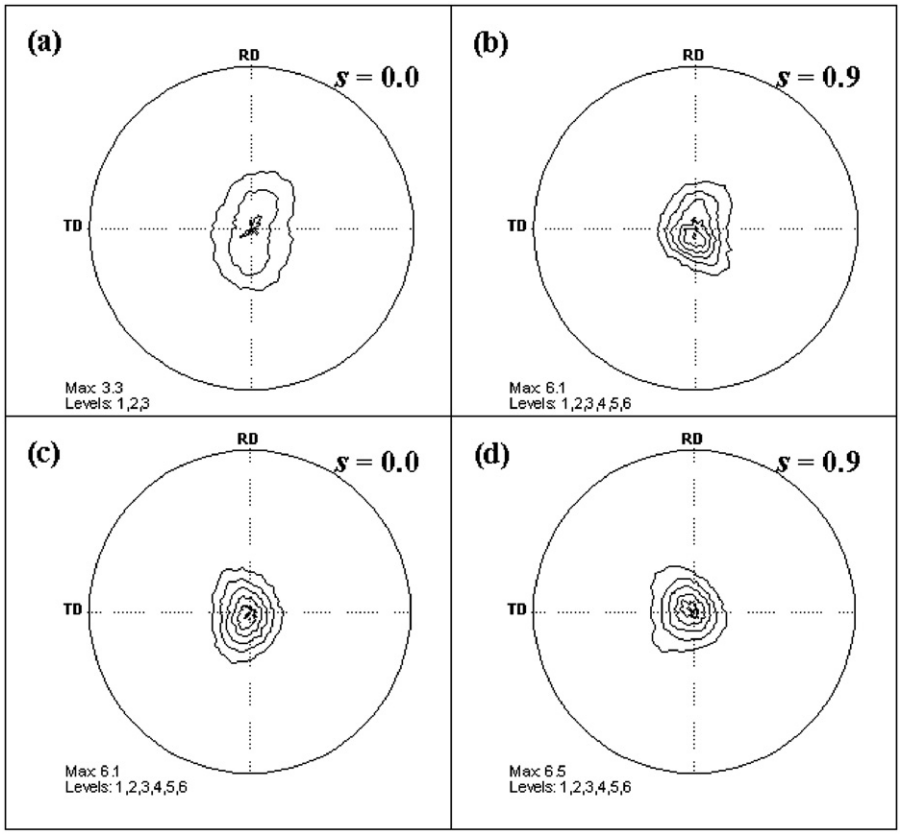

Fig. 7. (0 0 0 2) pole figures of the rolled AZ31 alloys after annealed at 673 K for 30 min: (a and b) normal rolling samples, and (c and d) cross-roll rolling samples ($s = 0.0$ is center layer; $s = 0.9$ is surface layer).

of the normal and cross-roll rolled sheets heat treated at 673 K for 30 min are 12.7 and 7.6 μm, respectively, indicating that the average grain sizes of the cross-roll rolled sample are smaller than those of the normal rolled sample.

Fig. 6 shows (0 0 0 2)//ND pole figure of the normal and cross rolled samples: (a) and (b) are normal rolling samples, and (c) and (d) are cross-roll rolling samples ($s = 0.0$ is center layer, $s = 0.9$ is surface layer). Texture development at the center layer of normal rolling sample was quite weak, because the sample was in the plane strain condition during rolling as analyzed in Fig. 4. However, the cross-roll rolled sample showed the formation of strong (0 0 0 2)//ND texture for the whole thickness of the sheet.

Fig. 7 shows (0 0 0 2)//ND pole figure after annealing at 673 K for 30 min of rolled samples: (a) and (b) are normal rolling samples, and (c) and (d) are cross-roll rolling samples ($s = 0.0$ is center layer, $s = 0.9$ is surface layer). It is specially noted that weakening of rolling texture was critically observed for the specimen center with normal rolling (Fig. 7(a)). While the texture gradient and intensity in the normal rolling sample decreased after annealing, the intensity difference between surface and center part of the sheet is still large. However, for the cross-roll rolled specimen, it is specially noted that the intensity of the texture is not severely different for the surface and center part, and thus the developed homogeneity of the (0 0 0 2) texture processed by cross-roll rolling can induce high formability, compared with the sheet with conventional rolling.

Fig. 8(a) and (b) shows normally rolled sample and cross-roll rolled sample respectively, after deep drawing cup tests at 473 K. For the case of the normally rolled sheets deformed at 473 K, the drawn cup showed wrinkles on the deformed part. However, the cross-roll rolled sheets deformed at 473 K, showed wrinkle-free surfaces, indicating that the application of the cross-roll rolling process has a potential for providing excellent formability to Mg alloys.

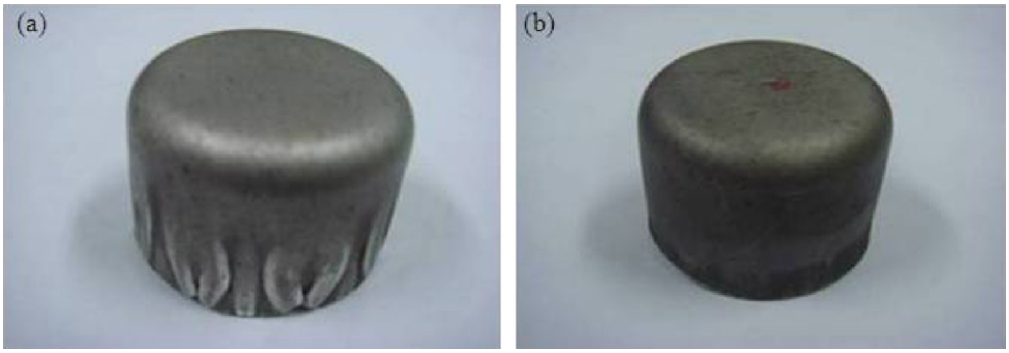

Fig. 8. The samples after the deep drawing cup test at 473 K: (a) normal rolled sample and (b) cross-roll rolled sample.

While further study is needed for identification of structural evolution depending on heat treatments, current observations clearly present that the cross-roll rolling can be one significant step for successful deformation process.

4. Conclusions

The evolution of strain states during cross-roll rolling and normal rolling was investigated by texture measurements and the three-dimensional finite element method simulation. Texture development at the center part of normal rolling sample is quite weak, because the sample was in the plane strain mode during rolling. However, the operation of the large $\dot{\varepsilon}_{23}$ during cross-roll rolling throughout the whole thickness layers leads to the formation of the weak deformation texture in the cross-roll rolled sample. The cross-roll rolled sample showed the formation of strong (0 0 0 2)//ND texture through the whole thickness of the sheet. For the texture gradient in the normal rolling sample, the intensity is decreased after annealing. However, the intensity of (0 0 0 2) basal texture of cross-roll rolled sample is decreased after annealing but homogeneous through the whole thickness of the sheet. Thus, the cross-roll rolled sample improved to have higher formability due to the homogeneity through the thickness of the sheet.

References

[1] G. Cole, Proceedings of the 56th Annual Meeting of IMA, Rome, Italy, June 6–8, 1999.
[2] E. Aghion, B. Bronfin, Mater. Sci. Forum 350–351 (2000) 19–30.
[3] J. Kaneko, M. Sugamata, M. Numa, Y. Nishikawa, H. Takada, J. Jpn. Inst. Met. 64 (2000) 141–147.
[4] F.C. Frank, J.F. Nicholas, Philos. Mag. 44 (1953) 1213–1235.
[5] R.B. Price, in: G. Thomas, J. Washburn (Eds.), Electron Microscopy and Strength of Crystals, Interscience Publishers, New York, NY, 1963, pp. 41–130.
[6] H.S. Lee, J.S. Park, Y.W. Chang, J. Mater. Process. Technol. 187–188 (2007) 550–554.
[7] H. Nishimura, O. Hasegawa, N. Koiso, K. Matsumoto, J. Jpn. Inst. Light Met. 53 (2003) 302–308.
[8] S.R. Agnew, O. Duygulu, Int. J. Plast. 21 (2005) 1161–1193.
[9] Y. Chino, K. Sassa, A. Kamiya, M. Mabuchi, Mater. Sci. Eng. A 441 (2006) 349–356.
[10] X.S. Huang, K. Suzuki, A. Watazu, Mater. Sci. Forum 544–545 (2007) 283–286.
[11] H. Watanabe, T. Mukai, K. Ishikawa, J. Mater. Sci. 39 (2004) 1477–1480.
[12] F.Z. Hassani, M. Ketaschi, Mater. Sci. Eng. A 528 (2011) 6426–6431.
[13] A.K. Singh, R.A. Schwarzer, Z. Metallkd. 96 (2005) 345.
[14] Y. Chino, J.S. Lee, K. Sassa, A. Kamiya, M. Mabuchi, Mater. Lett. 60 (2006) 173–176.
[15] Y. Chino, K. Sassa, A. Kamiya, M. Mabuchi, Mater. Lett. 61 (2007) 1504–1506.
[16] Y. Chino, K. Sassa, A. Kamiya, M. Mabuchi, Mater. Sci. Eng. A 473 (2008) 195–200.
[17] H.K. Lim, J.Y. Lee, D.H. Kim, W.T. Kim, J.S. Lee, D.K. Kim, Mater. Sci. Eng. A 506 (2009) 63–70.
[18] Y. Chino, K. Sassa, M. Mabuchi, J. Mater. Sci. 44 (2009) 1821–1825.
[19] J.J. Nah, H.G. Kang, M.Y. Huh, O. Engler, Scr. Mater. 58 (2008) 500–503.
[20] H.G. Kang, J.K. Kim, M.Y. Huh, O. Engler, Mater. Sci. Eng. A 452 (2007) 347–358.
[21] O. Engler, M.Y. Huh, C.N. Tomé, Metall. Mater. Trans. 36 (2005) 3127–3140.